The Wedge Splitting Test: Influence of Aggregate Size and Water-to-Cement Ratio

Pease, Bradley Justin; Skocek, Jan; Geiker, Mette Rica; Weiss, Jason; Stang, Henrik

Published in:
Proceeding of the RILEM Transport Mechanisms in Cracked Concrete Workshop

Publication date:
2007

THE WEDGE SPLITTING TEST: INFLUENCE OF AGGREGATE SIZE AND WATER-TO-CEMENT RATIO

Brad J. Pease (1), Jan Skoček (1), Mette R. Geiker (1), Henrik Stang (1), and Jason Weiss (2)

(1) Technical University of Denmark, Department of Civil Engineering, Lyngby, Denmark

(2) Purdue University School of Civil Engineering, West Lafayette, Indiana, USA

Abstract

Since the development of the wedge splitting test (WST), techniques have been used to extract material properties that can describe the fracture behavior of the tested materials. Inverse analysis approaches are commonly used to estimate the stress-crack width relationship; which is described by the elastic modulus, tensile strength, fracture energy, and the assumed softening behavior. The stress-crack width relation can be implemented in finite element models for computing the cracking behavior of cementitious systems.

While inverse analysis provides information about the material properties of various concrete mixtures there are limitations to the current analysis techniques. To date these techniques analyze the result of one WST specimen, thereby providing an estimate of material properties from single result. This paper utilizes a recent improvement to the inverse analysis technique, which enables the stress-crack width response to be determined simultaneously from multiple experimental tests. The effect of water-to-cement ratio and aggregate size are discussed. A comparison of epoxy-impregnated cracked WST specimen and material properties indicate a relationship between fracture properties and characteristics of load induced cracks.

Corresponding author's e-mail: bjp@byg.dtu.dk

Corresponding author's fax:+45 4588 3282

1. INTRODUCTION

The cohesive crack model is commonly applied to quasi-brittle materials such as concrete. The concept of the cohesive crack approach deviates from linear elastic fracture mechanics and considers that stresses can be transferred across the fractured surfaces. This transfer of stresses was first seen in steel in the form of plasticity [**1**,**2**] and was later applied to concrete with the concept of strain softening in [**3**]. The transfer of stresses in cracked concrete is illustrated in Figure 1a, and a generic cohesive law, or softening behavior (which can be readily applied in FEM programs) is shown in Figure 1b.

The wedge splitting test (WST) was created in [**4**] and further developed in [**5**] as a tool to determine the fracture of concrete or other cementitious materials. More recently, through the application of suitable analytical or finite element models, additional information including the estimated direct tensile strength, elastic modulus, and the cohesive law can be determined [**6**,**7**,**8**,**9**]. In [**9**] an analytical solution for the WST was determined using the hinge cracking model developed in [**10**]; however, several limitations existed. Included in these limitations are that only bi-linear cohesive laws could be determined and the inverse analysis could be conducted on a single test result. An iterative approach was developed in [**11**], which is described in greater detail in a following section. This iterative approach can be used to provide *N*-linear cohesive laws, however the inverse analysis is still conducted on a single experimental result.

The purpose of this paper is to investigate the effect to varying material parameters on the fracture behavior as determined by the WST and inverse analysis. A method to consider multiple experimental results in the inverse analysis approach is used. The effect of aggregate size, water-to-cement ratio, and cyclic loading is discussed. In addition, image analysis of cracked epoxy-impregnated specimens provides insight on the effect of changing fracture parameters on the characteristics of the cracks formed in concrete.

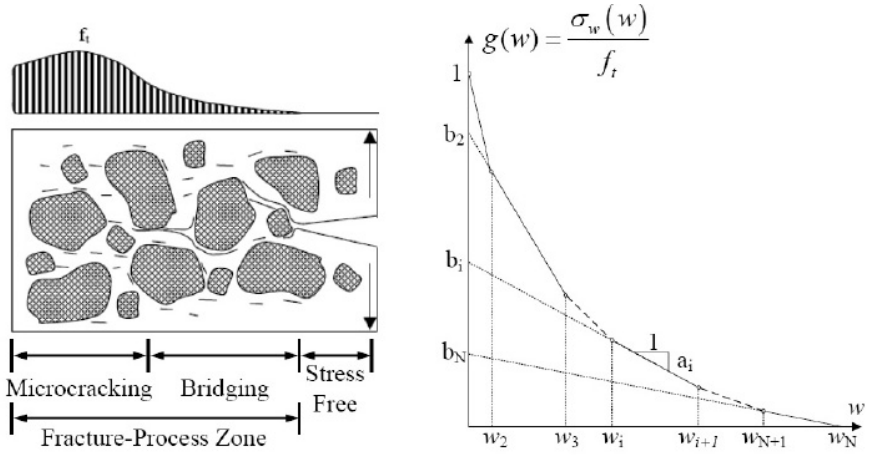

Figure 1. Illustrations of (a) concrete crack development with a fracture-process zone consisting of a bridging and microcracking regions (after [**12**]) and (b) the multi-linear softening behavior of cracked concrete.

Corresponding author's e-mail: bjp@byg.dtu.dk
Corresponding author's fax:+45 4588 3282

2. EXEPERIMENTAL DESCRIPTION

2.1 Mixture Proportioning and Specimen Preparation

Table 1 describes the mixture proportions used for testing, which included mixtures with varying maximum aggregate size and water-to-cement ratio (w/c). The concrete mixtures contained 65% aggregate by volume, with equal portions of graded sand and granite aggregate. The mortar mixture contained identical proportions of aggregate as the concrete mixtures, minus the coarse granite aggregate (i.e., 32.5% graded sand by volume). Aalborg Portland Basis© cement designated CEM II/A-LL 52.5 was used for all mixtures.

A conventional pan mixer was used for mixing 60 liter batches. The aggregate, half of the sand, water and cement were added to the mixer followed by the remaining sand. Mixing took place for 2 minutes, followed by a 2 minute rest period, and finally an additional minute of mixing. After mixing the concrete was placed and vibrated in 100 x 100 x 100 cube molds which contained a 20 mm x 30 mm plastic block to create a recess. The samples were cured in laboratory conditions, covered with plastic sheets for 24 hours. After this time the specimen we removed from the molds and were submerged in lime-saturated water at 20°C until testing at 1, 3, 5, 7, 14, and 21 days. Immediately prior to testing a 30 mm deep notch was cut into the specimen using a concrete saw. Figure 2 and 3 provide illustrations of the final specimen geometry after saw cutting. Additional information on the mixing procedure can be found in [**13**].

Table 1. Mixture Proportions and Descriptions

Mixture ID	w/c	Description	Max. Size Aggregate (mm)
A	0.42	Large Aggregate Concrete	16
B	0.42	Small Aggregate Concrete	8
C	0.42	Mortar	4
E	0.34	Paste	--
G	0.50	Large Aggregate Concrete	16
H	0.30	Large Aggregate Concrete	16

2.2 Wedge Splitting Test and Inverse Analysis

The WST experimental setup is shown in Figure 2. During testing, a splitting load is applied to a concrete specimen through a rigid wedge and bearing plates with low-friction rollers. The specimen consists of a 100 x 100 x 100 mm cube with a 20 mm deep by 30 mm wide recess, which allows for application of the splitting load.

The WST can be used, through inverse analysis (e.g., minimizing the difference between the model calculations and experimental results by altering mechanical parameters), to determine the cohesive law for cementitious composites. Figure 3 shows the implementation of the hinge model developed in [**14**,**10**] to the WST geometry. The hinge model simulates the area directly surrounding a propagating crack, which are attached to rigid boundaries. The rigid boundaries of the cracked hinge are allowed to translate and rotate as indicated in Figure 3b. The rigid boundaries seamlessly join the bulk (uncracked) specimen, where the behavior is controlled by the classical elastic theory (i.e. Hooke's Law).

Corresponding author's e-mail: bjp@byg.dtu.dk

Corresponding author's fax:+45 4588 3282

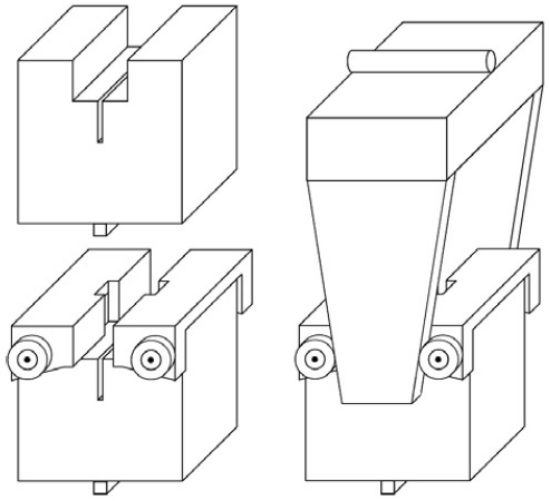

Figure 2. Schematic of WST geometry: Specimen is placed on line support, two roller bearing loading devices are mounted, and wedge applies splitting load [**9**].

The stresses transferred in the hinge model are controlled by Equation 1

$$\sigma = \begin{cases} \sigma(\varepsilon) = E\varepsilon & \text{Precracked State} \\ \sigma_w(w) = g(w) f_t & \text{Cracked State} \end{cases} \qquad \text{Equation 1}$$

where E is the elastic modulus, ε is the elastic strain, $\sigma_w(w)$ represents the cohesive law, and f_t is the uniaxial tensile strength. Figure 1b illustrates a general $g(w)$ curve, which mathematically is given by

$$g(w) = b_i - a_i w \text{ where } w_{i-1} < w < w_i \text{ and } i = 1 \to N . \qquad \text{Equation 2}$$

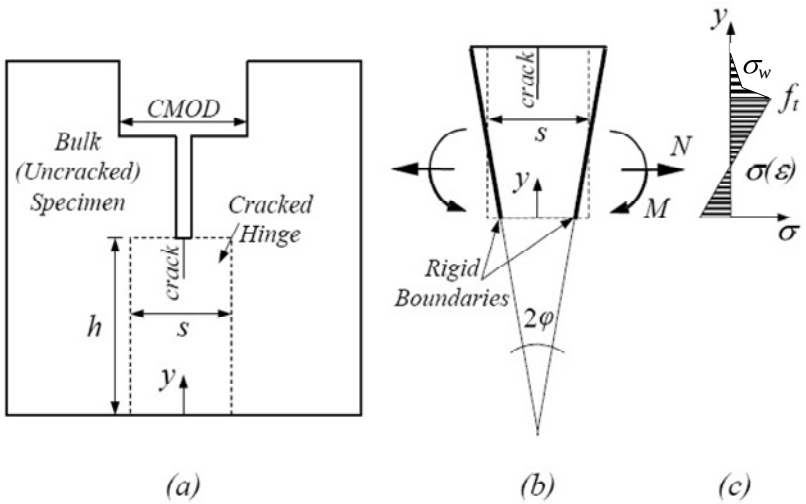

Figure 3. (a) The wedge split testing specimen with the hinge model applied, (b) Loading and deformation of the hinge (after [**10**]), and (c) the assumed stress distribution (after [**10**]).

Corresponding author's e-mail: bjp@byg.dtu.dk

Corresponding author's fax:+45 4588 3282

The term w_i is the intersection of two consecutive lines and is computed by

$$w_i = \frac{b_i - b_{i+1}}{a_i - a_{i+1}} \text{ where } i < N,$$

and the critical crack width (width at which $g(w) = 0$) is calculated by

$$w_c = w_N = \frac{b_N}{a_N}$$

where N is equal to the number of lines in the cohesive law. The deformation of the hinge is determined by the angular rotation, φ and the location of the neutral axis, y_0 (see Figure 3). The mean value of longitudinal strains, $\varepsilon^*(y)$ is calculated by Equation 3.

$$\varepsilon^*(y) = (y - y_0)2\varphi / s \qquad \text{Equation 3}$$

The deformation of an incremental strip of the hinge is then given by $u(y) = s \cdot \varepsilon^*(y)$, where s is the length of the hinge ($s = 0.5h$). Once cracking occurs, $u(y)$ can be computed as the sum of the elastic deformation and the crack opening, as shown in Equation 4.

$$u(y) = s \cdot \varepsilon^*(y) = s\frac{\sigma_w(w(y))}{E} + w(y) \qquad \text{Equation 4}$$

By combining Equation 3 and 4 the stress distribution as seen in Figure 3c is mathematically written as follows in Equation 5

$$\sigma_w(w(y)) = (2(y - y_0)\varphi - w(y))\frac{E}{s} \qquad \text{Equation 5}$$

and by introducing the cohesive law (Equation 1) and solving with respect to $w(y)$ and $\sigma_w(w(y))$ the following solutions are obtained:

$$\sigma_w(w(y)) = \frac{\zeta - 2\varphi(y - y_0)\beta_{i\,i}}{1 - \beta_i}\frac{E}{s} \qquad \text{Equation 6}$$

$$w(y) = \frac{2\varphi(y - y_0) - \zeta_i}{1 - \beta_i} \qquad \text{Equation 7}$$

where the dimensionless factors β_i and ζ_i are defined by

$$\beta_i = \frac{f_t a_i s}{E} \text{ and } \zeta_i = \frac{f_t b_i s}{E}. \qquad \text{Equation 7a}$$

Additional information on the development and implementation of the hinge model can be found in [**10**] and [**9**,**15**,**11**], respectively.

In [**9**] the hinge model was applied to the WST geometry and an analytical solution was utilized to determine a bilinear cohesive law. An iterative approach was developed in [**11**] which allows for determination of N-linear cohesive laws. The following section provides an

overview of the iterative inverse analysis technique for determination of *N*-linear cohesive laws.

The inverse analysis proceeds based upon the following two main equations:

$$M_{\exp} - M_{Hinge} = 0 \quad \text{and} \quad CMOD_{\exp} - CMOD_{Hinge} = 0 \qquad \text{Equation 8}$$

where M_{exp} is the bending moment applied during experimental testing, M_{Hinge} is the bending moment applied in the hinge model approach, $CMOD_{exp}$ is the observed CMOD from experiments, and $CMOD_{Hinge}$ is the CMOD computed from the hinge model. The experimental bending moment, M_{exp} is computed by

$$M_{\exp} = P_{sp}\left(d_2 - y_0\right) + \frac{1}{2}P_v d_1 + \frac{1}{2}mge \qquad \text{Equation 8a}$$

where

$$P_v = P_{sp}\frac{2\tan\alpha_w + \mu_c}{1 - \mu_c \tan\alpha_w} \qquad \text{Equation 8b}$$

which accounts for the wedge angle, α_w and the friction in the roller bearings, μ_c; m is the mass of the specimen and g is the acceleration of gravity. The bending moment applied in the hinge model, M_{Hinge} is computed by

$$M_{Hinge} = \int_0^h \sigma(y)(y - y_0)dy \qquad \text{Equation 8c}$$

where $\sigma(y)$ is the cohesive law from Equation 1. The CMOD calculated by the hinge model, $CMOD_{Hinge}$ is the sum of the elastic deformation, δ_e; the deformation caused by the crack, δ_w; and the deformation caused by geometrical amplification, δ_g. The calculation of the elastic deformation, δ_e is found in [**16**] as

$$\delta_e = \frac{P}{Et}\upsilon_2 . \qquad \text{Equation 8d}$$

Here t is the specimen thickness and υ_2 is computed by [**16**]:

$$\upsilon_2 = \frac{x}{(1-x)^2}\left[38.2 - 55.4x + 33.0x^2\right] \qquad \text{Equation 8e}$$

The deformation caused by the crack, δ_w can be directly calculated from Equation 7 at $y = h$. Finally, the deformation caused by geometrical amplification, δ_g is computed by

$$\delta_g = 2(b-h)\left(\frac{\delta_w}{2d} - \frac{\varphi_e}{1-\beta_i}\right) \qquad \text{Equation 8f}$$

where φ_e is defined as the maximum elastic angular deformation of the hinge and d is the depth to which the crack has propagated through the hinge.

An analytical solution to Equation 8 cannot be obtained and therefore an optimization process has been implemented using MatLab. This process minimizes the difference between the observed load applied in experiments, P_{exp} and the load predicted by the hinge model, P_{Hinge} using the following error normalization function:

$$\left\| P_{\exp} - P_{Hinge} \right\| = \sqrt{1 + \frac{\left(P_{\exp} - P_{Hinge}\right)^2}{2}} - 1 \qquad \text{Equation 9}$$

Corresponding author's e-mail: bjp@byg.dtu.dk
Corresponding author's fax:+45 4588 3282

This normalization function is applied to various stages of the load response curves, including the elastic portion for determination of E, the peak load for determination of f_t, and the softening branch for determination of a_i and b_i. Additional information on this optimization process, including a parametric study and method of implementation in Matlab can be found in [**11**].

Previously, this and similar inverse analysis approaches have been used to fit results from single experimental data [**9**,**15**,**11**], however experimental results tend to vary slightly from test to test. Therefore, in order to allow for fitting from multiple specimen the following modification has been made, which minimizes the difference between the hinge model curve and a multitude of experimental curves.

$$\min = \sum_{i=1}^{N_{\exp}} \left[\left(\sum_{j=1}^{N_p} \sqrt{1 + \frac{\left(P_{\exp}^{i,j} - P_{Hinge}^{i,j}\right)^2}{2}} - 1 \right) \Big/ N_p \right] \qquad \text{Equation 10}$$

for $i=1$ *to* N_{exp}, where N_{exp} is the number of experimental curves and for $j=1$ *to* N_p where N_p is the number of data points in the individual experimental curve. By dividing by the number of data points, N_p in the individual curves, the data is normalized by the number of points; therefore, not overemphasizing the effect of a single curve on the overall fitting of the hinge model. Figure 4a shows multiple experimental WST results from a single concrete batch along with the results of the inverse analysis. It can be seen that the inverse analysis is averaging the behavior of the multiple tests.

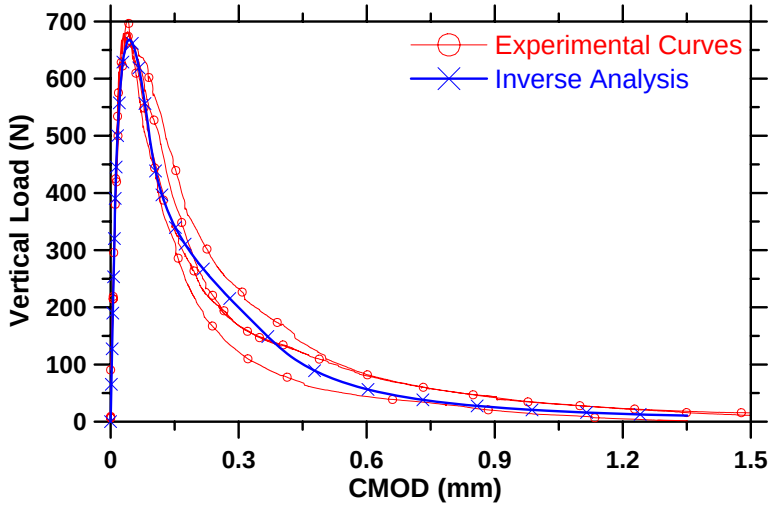

Figure 4. Results of inverse analysis of multiple WST specimen

2.3 Crack Impregnation and Image Analysis

A fluorescent dye epoxy was used for impregnation of cracked WST specimen at varying crack mouth opening displacements (CMOD). The WST specimens were loaded to a specific CMOD and then epoxy impregnated under vacuum. After hardening of the epoxy the samples were cut using a diamond saw. Images were taken of the impregnated samples under a UV-light source which causes the epoxy to illuminate, simplifying the image analysis

Corresponding author's e-mail: bjp@byg.dtu.dk
Corresponding author's fax:+45 4588 3282

process. A semi-automated image analysis technique was used to convert the images into black and white (solid concrete presented in black, crack(s) in white) and various masks were applied to determine geometrical characteristics of the cracks. Additional information on the epoxy impregnation and semi-automated image analysis techniques can be found in [**17**] and [**18**], respectively.

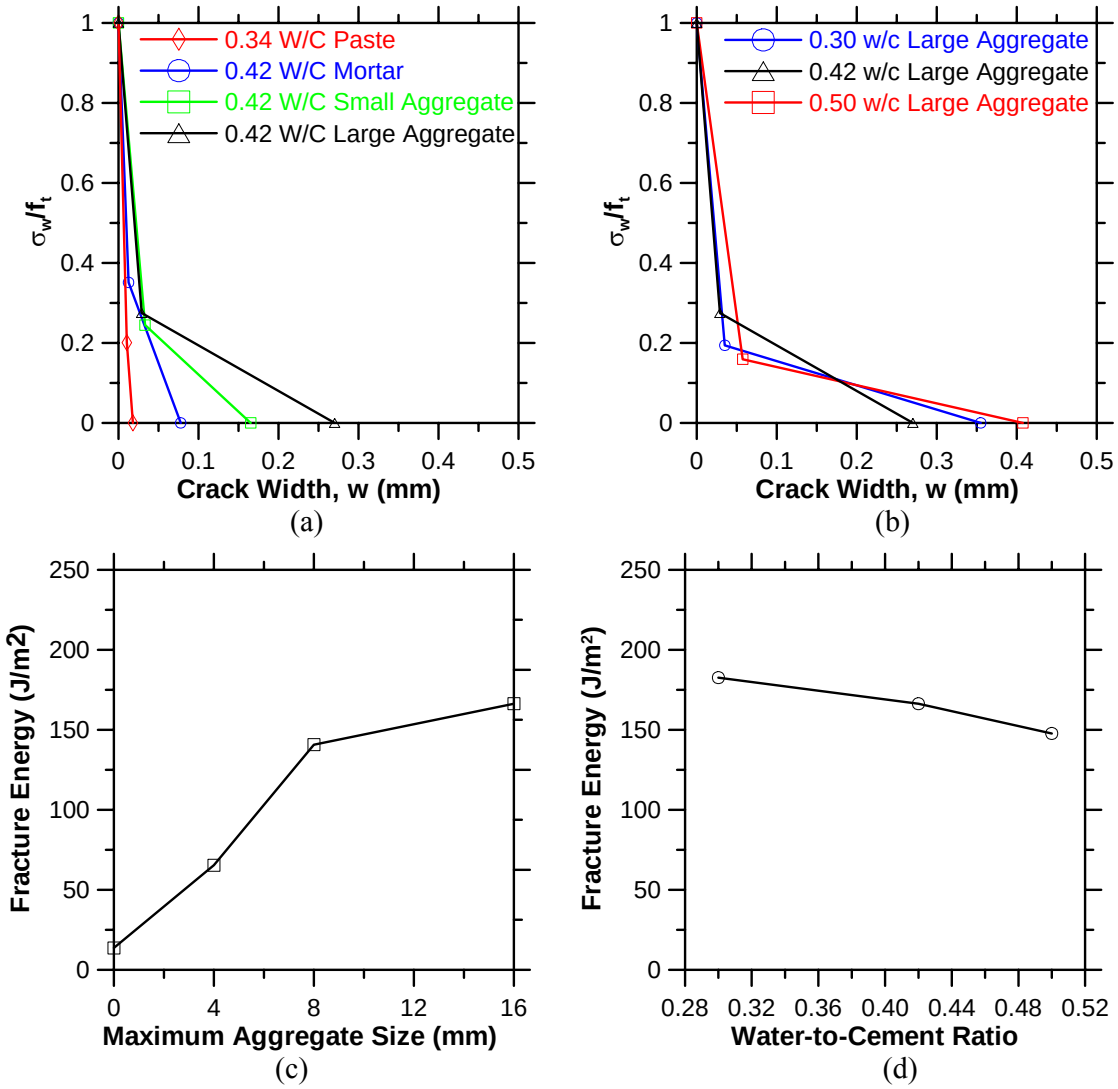

Figure 5. The effect of aggregate size on the (a) cohesive law and (c) fracture energy, and the effect of w/c on the (b) cohesive law and (d) fracture energy for all mixtures at age of 14 days.

3. RESULTS AND DISCUSSION

3.1 Inverse Analysis Results

The results of the inverse analysis of the various concrete mixtures are presented in Figure 5. In this case the results of a bi-linear cohesive law inverse analysis are presented. Figure 5a illustrates the effect of increasing the maximum aggregate size on the transfer of stresses

Corresponding author's e-mail: bjp@byg.dtu.dk
Corresponding author's fax:+45 4588 3282

across a crack. The paste mixture transfers only minimal stresses after cracking, while the stresses transferred across the crack increases with an increase in the size of the maximum aggregate. The effectiveness of the aggregate to transfer stresses can be quantified by the critical crack width, or the crack width where stress transfer ceases. The critical crack width of the paste is approximately 0.02 mm, while the concrete with 16 mm aggregate has a value of approximately 0.27 mm. The increase in stress transfer and critical crack width is typically attributed to aggregate interlock and friction between the fracture surfaces [**19**]. Figure 5c shows the effect of the maximum aggregate size on the fracture energy (paste is assumed to have maximum aggregate size of 0 mm). The effect of aggregate size on increasing the fracture energy is clearly illustrated. The fracture energy increases from 13.7 J/m^2 for the cement paste to 166 J/m^2 for the large aggregate concrete. It should be noted that the paste used in this investigation had a different w/c than the concrete and mortar mixtures. The 0.34 w/c paste was selected, based on the estimations in [**20**], to assess the properties of the paste if the effects of the interfacial transition zone were not considered. However, as presented below, the effect to of w/c is relatively minor; therefore it is reasonable to assume a similar result would be obtained from a 0.42 w/c paste.

The effect of w/c on the cohesive laws and fracture energy are shown in Figure 5b and d, respectively. Figure 5b shows that the w/c has a relatively minor effect on the cohesive law as compared aggregate size. The effect of w/c on the fracture energy is plotted in Figure 5d. The fracture energy increases 24% by decreasing w/c from 0.50 to 0.30. Similar results have been seen previously (for example [**6**,19]). The same reduction in w/c caused a 49% increase in stiffness and a 45% increase in tensile strength. Additionally, the effect of age was investigated. Results indicated increases in elastic modulus and tensile strength with time; however, fracture energy varied only slightly with time.

Figure 6 shows the results of the epoxy impregnation of the cracked WST specimens. The area of the crack was determined using image analysis software, and has been plotted versus the CMOD for the 0.42 w/c concrete with small and large aggregate (8 mm and 16 mm maximum size aggregate). Figure 6 shows that the small aggregate concrete developed cracks with a larger crack area for a particular crack width than the large aggregate cracks with a

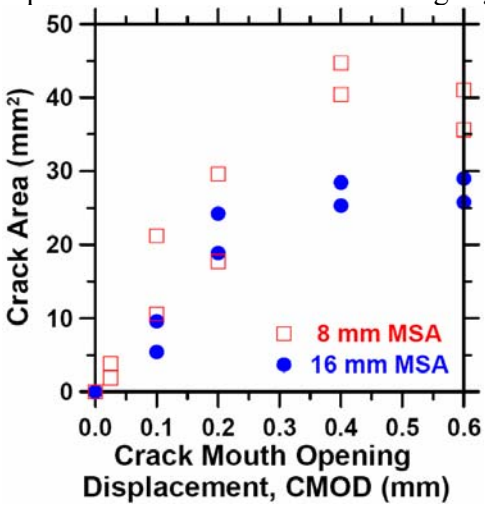

Figure 6. The resulting crack area from varying CMOD's for the 0.42 w/c concrete with 8 mm (small) and 16 mm (large) maximum sized aggregate (MSA) [**21**].

Corresponding author's e-mail: bjp@byg.dtu.dk
Corresponding author's fax:+45 4588 3282

larger crack area for a particular crack width than the large aggregate concrete. As shown in Figure 5a and c the stress transfer and fracture energy increase as the maximum aggregate size increases. The ability of the larger aggregate concrete to transfer stresses at larger crack widths allows this material to restrict the opening of the crack, and therefore maintaining a smaller crack area.

3.2 Unloading Stiffness of the Wedge Splitting Test

Figure 7 shows the result of cyclic load application to a single wedge splitting specimen of Mixture A. The specimen was unloading in both the pre- and post- peak portions of loading, and the load and CMOD have been normalized to the peak vertical load (1500 N) and the corresponding CMOD (0.042 mm). The slopes of the individual unloading responses converge on a common point, referred to as the focal point (σ_0,ε_0), which is shown in Figure 7a. As discussed at greater length in [**22**,**23**] the focal point allows for the determination of the stiffness at any point along the envelope of the load-CMOD response. Figure 7b shows the degrading effect of increasing crack width on the original stiffness, $E_{Original}$. A 1% reduction in stiffness occurred after loading to 47% of the peak load. The degradation of stiffness then increases rapidly, resulting in a 38% reduction in stiffness at peak loading (i.e., normalized CMOD equal to 1). The stiffness continues to degrade with increasing crack width.

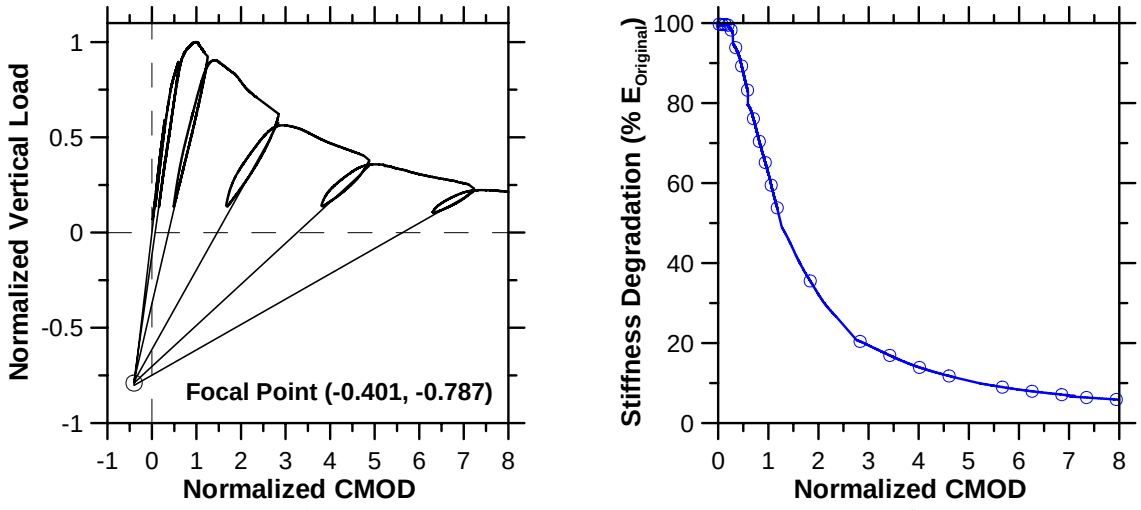

(a) (b)

Figure 7. (a) Cyclic loading of the WST indicates a focal point, and (b) the unloading stiffness degradation

4. SUMMARY

This paper has shown that the wedge splitting test specimen geometry can be used to determine material properties that can describe the fracture behavior of concrete. It has been shown that:

Corresponding author's e-mail: bjp@byg.dtu.dk
Corresponding author's fax:+45 4588 3282

- The use of the normalization function presented in Equation 10 makes it possible to perform a simultaneous inverse analysis on multiple test specimens.
- The inclusion of aggregate resulted in an order of magnitude increase in fracture energy. The critical crack width and the fracture energy increased with the maximum aggregate size. The fracture energy for the large aggregate concrete was 12 times higher than for cement paste. This increase is attributed to the increase in aggregate interlock and friction between fracture surfaces.
- While varying the water-to-cement is typically thought to have a major influence on mechanical properties, the fracture energy and cohesive laws are only slightly affected by such variations. The fracture energy varied only 24% for the water-to-cement ratios used.
- Epoxy impregnation of cracked WST specimen indicates links between the fracture properties and the geometric characteristics of the cracks. It was seen that increasing the fracture energy results in a less tortuous crack geometry.
- The slopes of the individual unloading responses from a cyclic wedge splitting test converge at a focal point, similarly to compression and direct tension results from previous investigations. The focal point allowed for the determination of the stiffness at any point along the vertical load-CMOD curve. The stiffness of the wedge split test specimen rapidly degraded after reaching approximately 47% of the peak load.

ACKNOWLEDGEMENTS

The authors gratefully acknowledge the support provided by the Knud Højgaard Foundation. Additionally, the last author acknowledges the National Science Foundation (Grant No. 0134272) for support. Any opinions, findings, and conclusions or recommendations expressed in this material are those of the author(s) and do not necessarily reflect the views of the research sponsors.

REFERENCES

[1] Dugdale, D. S. (1960) *Journal of the Mechanics and Physics of Solids***8**, 100–104.

[2] Barenblatt, G. I. (1962) *Advances in Applied Mechanics***7**, 55–129 Originally Published in Russian, See e.g. Karihaloo 1995.

[3] Hillerborg, A., Modéer, M., and Petterson, P. (1976) *Cement and Concrete Research***6**, 773–781.

[4] Linsbauer, H. and Tschegg, E. (1986) *Zement und Beton***31**, 38–40.

[5] Brühwiler, E. and Wittman, F. H. (1990) *Engineering Fracture Mechanics***35**, 117–125.

[6] Wittmann, F. H., Roelfstra, P. E., Mihashi, H., Huang, Y.-Y., Zhang, X.-H., and Nomura, N. (1987) *Materials and Structures***20(116)**, 103–110.

[7] Ulfkjær, J. and Brincker, R. (1993) In Fracture and Damage of Concrete and Rock – FCDR-2 : E & FN Spon pp. 135–144.

[8] Kitsutaka, Y. (1997) *Journal of Engineering Mechanics - Proceedings of the ASCE***123(5)**, 444–450.

[9] Østergaard, L. Early-Age Fracture Mechanics and Cracking of Concrete - Experiments and Modeling PhD thesis Technical University of Denmark Lyngby, Denmark (2003).

Corresponding author's e-mail: bjp@byg.dtu.dk
Corresponding author's fax:+45 4588 3282

[10] Olesen, J. F. (2001) *Journal of Engineering Mechanics - Proceedings of the ASCE***127(3)**, 272–280.

[11] Skocek, J. and Stang, H. (2007) *Submitted to Engineering Fracture Mechanics*.

[12] vanMier, J. G. M. (1997) Fracture Processes in Concrete Assessment of Material Parameters for Fracture Models, CRC Press, .

[13] Weiss, W. J., Geiker, M. R., and Hansen, K. K. (2007) *Submitted to Journal of Testing and Evaluation*.

[14] Ulfkj$æ$r, J. P., Krenk, S., and Brincker, R. (1995) *Journal of Engineering Mechanics***121(1)**, 7–15.

[15] Löfgren, I., Stang, H., and Olesen, J. F. (2005) *Journal of Advanced Concrete Technology***3(3)**, 423–434.

[16] Tada, H., Paris, P. C., and Irwin, G. R. (1985) The Stress Analysis of Cracks Handbook, Paris Productions Incorporated, 226 Woodbourne Dr., St. Louis, Missouri, USA.

[17] Laugesen, P. June 2005 In Proceedings of the Knud Højgaard Conference Advanced Cement-Based Materials – Research and Teaching Lyngby, Denmark: . .

[18] Qi, C., Weiss, W. J., and Olek, J. (2003) *Concrete Science and Engineering***36(260)**, 386–395.

[19] Shah, S. P., Swartz, S. E., and Ouyang, C. (1995) Fracture Mechanics of Concrete, John Wiley & Sons, Inc., .

[20] Bentz, D., Detwiler, R., Garboczi, E., Halamickova, P., and Schwartz, L. (1997) In L.O. Nilsson and J.P. Ollivier, (ed.), Proceedings of Chloride Penetration into Concrete, RILEM : .

[21] Weiss, J. and Geiker, M. The influence of cracks on concrete Presentation at ACI Spring Meeting April 24 2007.

[22] Puri, S. and Weiss, J. (2006) *Journal of Materials in Civil Engineering***18(3)**, 325–333.

[23] Yankelevsky, D. Z. and Reinhardt, H. W. (1987) *ACI Materials Journal***84(5)**, 365–373.

Corresponding author's e-mail: bjp@byg.dtu.dk
Corresponding author's fax:+45 4588 3282